JOURNAL OF MATERIALS SCIENCE 30 (1995) 1046–1052

Elevated temperature X-ray measurement of residual stresses in a fibre reinforced Al alloy

ANDERS WEILAND*, TORSTEN ERICSSON
Division of Engineering Materials, Department of Mechanical Engineering, Linköping University, S-581 83 Linköping, Sweden

Thermal residual stresses have been measured using X-ray diffraction in an Al–2% Mg matrix with 10, 20 or 26 vol % Al_2O_3 short fibres. Stress measurements were made at room temperature as well as *in situ* at elevated temperatures up to 250 °C. The thermal stresses arise due to the difference in coefficient of thermal expansion (CTE) between the matrix and the reinforcement. The largest CTE is found in the matrix, resulting in tensile residual stresses after a temperature drop, e.g. after processing or annealing. A high fraction of reinforcement implies higher matrix stresses than a low fibre content. The stresses decrease with increasing temperature for all fibre volume fractions. Measurements are compared with calculations using a modified Eshelby model for equivalent inclusions. Parameters taken into account in the model are coefficient of thermal expansion, Young's modulus, and volume fraction and geometric shape of the reinforcing phase. A good correlation between calculations and experimental results has been found, bearing in mind that no plasticity is taken into account in the Eshelby model. The plastic behaviour of the composites has been described using a model based on a rigid spherical cavity in an elastic–plastic matrix.

1. Introduction

In aluminium alloys, several advantages may be gained by the introduction of ceramic reinforcement, e.g. increased resistance to erosion and wear, improved strength and better dimensional stability under temperature variations. The maximum service temperature may be increased with retained mechanical properties. Hence, these composites are strong candidates in applications where increased service temperature would be desirable, but where the hitherto used alloys do not meet the new requirements.

Due to the difference in coefficients of thermal expansion (CTE) between the matrix and the reinforcing phase of a metal matrix composite, large thermal misfit strains (and stresses) arise in the material during cooling from process temperature. The magnitude of the stresses depends on the matrix–reinforcement system and on the thermal history of the composite. These stresses may be detrimental to the mechanical properties of the composite, especially since the largest CTE of the phases is found in the matrix, giving rise to tensile residual stresses in the matrix. Typically, the matrix CTE is some four to seven times that of the reinforcement.

Numerous investigations of residual stresses in a wide variety of matrix–reinforcement systems have been made using X-ray or neutron diffraction. Practically all of these measurements have been made at room temperature. Since many metal matrix composites (MMCs) are potential elevated temperature materials, the need for residual stress determination at higher temperatures is obvious. In order to meet this demand, a device has been built by which *in situ* X-ray diffraction measurements of residual stresses at elevated temperatures can be conducted [1]. Measurements using this device have been made at four different temperatures between 25 and 250 °C. The aim of the work has been to study the formation and relaxation of residual stresses due to temperature changes and to describe the composite's behaviour using an elastic model, namely the modified Eshelby model for equivalent inclusions, as well as an elastic–plastic model where yielding of the matrix is taken into consideration.

2. Theory

2.1. Macro- and microstresses

Residual stresses can be divided into macrostresses and microstresses [2]. Macrostresses can be a result of mechanical deformation that causes plastic deformation in the surface layers of the material, such as shot-peening, grinding, machining, etc. Since the surface layers will also constrain the bulk in return, the bulk material will also have residual stresses even though it may not have suffered deformation. Thermal macro-stresses may be induced in a material during cooling from a process temperature or by various heat treatments. Different yield points in the different phases of a multiphase material cause an inhomogeneous partitioning of plastic strain between

* Formerly Ohlsson.

0022–2461

the phases, causing a residual microstress state to form due to the constraining effect of the stronger phase on the weaker.

For any residual stress, σ_{ij} in a two-phase material, it holds [2]

$$\int_D \sigma_{ij} \mathrm{d}D = \int_{D_m} \sigma_{ij} \mathrm{d}D_m + \int_{D_f} \sigma_{ij} \mathrm{d}D_f = 0 \quad (1)$$

where D_m and D_f are the respective volumes of the two phases, the matrix and the fibres of a composite for instance, and D is the total volume of the body. If $\langle\sigma_{ij}\rangle_m$ and $\langle\sigma_{ij}\rangle_f$ denote the average stresses in the two phases, and v_m and v_f are the volume fractions, Equation 1 can be written

$$v_m\langle\sigma_{ij}\rangle_m + v_f\langle\sigma_{ij}\rangle_f = 0 \quad (2)$$

These average microstresses can be determined experimentally by X-ray diffraction. The average is to be taken over a volume containing a statistically representative number of grains, and it is constant in a given phase as long as a representative volume is measured.

In polycrystalline materials, a large number of grains contribute to the information obtained by X-ray diffraction. Hence, the measured strains are average values. In order to determine the average stress from these strain values, average elastic constants are required. However, since the only diffracting grains are those whose normal bisect the incident and diffracting beams, the averaging is only over a particular set of grains, all of which have a specific form of lattice directions $\langle hkl\rangle$ in a particular orientation. Thus, an added constraint is required for the theoretical calculation of average stresses from the single crystal elastic constants, and the values ν/E and $(1+\nu)/E$ are no longer satisfactory [2]. Hence, the X-ray elastic constants, S_1^*, and $1/2S_2^*$ must be derived [3], e.g. assuming constant stress in all grains in accordance with the Reuss model.

2.2. The modified Eshelby model

Originally, this theory was presented in the late 1950s and early 1960s by Eshelby [4–6]. It has since then been successfully applied by numerous researchers to dispersion strengthened systems, as well as continuous fibre and short fibre reinforced composites, see [7–13].

An excellent description of a series of "cutting and welding exercises" illustrating the Eshelby method to calculate the stresses in a matrix with misfitting inclusions has been given by Withers *et al.* [11]. An inclusion with the *same* elastic constants as the matrix is cut from the unstressed material, and imagined to undergo a stress-free shape change by the transformation strain, $\boldsymbol{e}^T$. To facilitate refitting of the inclusion into the position from which it was cut, surface tractions are applied. Back in its place, the surface tractions are removed, and equilibrium is reached at a constrained strain, $\boldsymbol{e}^C$, of the inclusion relative to its initial shape.

For an ellipsoidal inhomogeneity, e.g. a fibre or whisker, embedded in an elastically homogeneous matrix and with elastic constants, $\mathbf{C}_I$, *different* from those of the matrix, a procedure similar to the above gives the valid equations. The stress-free strain mismatch can be considered as a transformation strain, $\boldsymbol{e}^{T*}$, of the inhomogeneity. Again, on replacing the inclusion in its hole, it takes up the constrained shape, $\boldsymbol{e}^C$. A second inclusion of the *same* elastic constants as the matrix can be imagined to undergo a stress-free transformation strain, $\boldsymbol{e}^T$, so that when surface tractions are removed and equilibrium is reached, it will have the same uniform stress state. The inhomogeneity with elastic constants, $\mathbf{C}_I$, and the equivalent inclusion with elastic constants, $\mathbf{C}_M$, can be interchanged without disturbing the matrix, since they, despite different strain states, have identical stress states.

For a material with a finite concentration of inclusions, *all aligned in the same direction*, one may, following Withers *et al.* [11], arrive at an expression for the mean matrix stress $\langle\sigma\rangle_M$ in the case of no externally applied stress

$$\langle\sigma\rangle_M = v_I\mathbf{C}_I\mathbf{C}_M(\mathbf{S}-\mathbf{I})\{(\mathbf{C}_M-\mathbf{C}_I) \times [\mathbf{S}-v_I(\mathbf{S}-\mathbf{I})]-\mathbf{C}_M\}^{-1}\boldsymbol{e}^{T*} \quad (3)$$

where v_I is the volume fraction of inclusions, $\mathbf{C}_I$ and $\mathbf{C}_M$ are the stiffnesses of the inclusion and matrix, respectively, $\mathbf{S}$ is the dimensionless Eshelby tensor, $\mathbf{I}$ the identity tensor, and $\boldsymbol{e}^{T*}$ the transformation strain. The Eshelby tensor, $\mathbf{S}$, is only dependent on the geometry, i.e. aspect ratio of the inclusion and the Poisson's ratio of the matrix. For the case of thermal stresses $\boldsymbol{e}^{T*}$ is given in terms of the difference $\Delta\alpha = \alpha_M - \alpha_I$ in coefficient of thermal expansion between the matrix and the inclusion multiplied by the appropriate temperature change, ΔT, [11], i.e.

$$\boldsymbol{e}^{T*} = (\alpha_M - \alpha_I)\Delta T \quad (4)$$

Explicit expressions for the components of the stiffness and Eshelby tensors for a number of geometries can be found in Mura [14] and in Taya and Arsenault [15]. If the inclusions are completely randomly distributed (rather than aligned) in the matrix, the tensor $(\mathbf{S}-\mathbf{I})$ in Equation 3 has to be replaced by an average Eshelby tensor $\langle\mathbf{S}\rangle$ is given by Li [16].

One may note that Equation 3 can be written $\langle\sigma\rangle_M = \boldsymbol{A}\,\boldsymbol{e}^{T*}$ where the tensor $\boldsymbol{A}$ is dependent only on the elastic constants of the phases, and the volume fraction and shape of the inclusion. It is also important to note that Equation 3 gives an approximation of the *mean* matrix stress in the case of a finite, i.e. real, composite. The reasons for concentrating on mean rather than local stresses are that it is the mean values that govern much of a composite's mechanical behaviour [11], and that diffraction techniques with X-ray or neutron radiation reveal the mean values, i.e. average microstresses (or strains), as discussed in Section 2.1.

3. Experimental procedure

3.1. Materials and heat treatment

The metal matrix composite system investigated is based on the alloy Al–2% Mg as matrix material. Three volume fractions, v_f = 10, 20 and 26 vol % (v/o),

of Al_2O_3 fibres were introduced by squeeze casting. The fibres are δ-Al_2O_3 short fibres of the Saffil type from ICI with average diameter 3 μm, randomly distributed in a plane. To structurally stabilize the fibres and to obtain a fine-grained microstructure in the fibres about 4% SiO_2 is incorporated. Silica is also used as binder in the preform, giving good handling strength and machinability [17]. In an investigation of this composite system by Liu *et al.* [18], it has been shown that the silica binder reacts strongly with the liquid alloy during fabrication of the composite. The binder transforms to spinel ($MgAl_2O_4$) and the silicon dissolves in the matrix and reacts with Mg to form intermetallic Mg_2Si precipitates. This can be seen in Fig. 1 where arrow A indicates the transformed binder and arrow B shows Mg_2Si. In [18] it is suggested that the Mg_2Si precipitates influence the mechanical properties, since remarkably high elongation values have been measured.

The as-cast material was cut into approximately 2 mm thick slabs for residual stress measurement. All samples were annealed in a small chamber furnace in air at 350 °C for 15 min, followed by free cooling in air. After this treatment it is reasonable to assume that the macrostresses are zero, since the cooling rate has been low and the samples are small enough to ensure a homogeneous temperature distribution throughout the sample volume.

To determine the stress free lattice spacing, d_0, powders were made from material will all three different fibre volume fractions. The three materials were ground on 500 mesh SiC paper, giving ultrafine powders. These powders were heat treated at 300 °C in air for 30 min and air cooled, ensuring that any microstresses possibly arisen during grinding were fully relaxed.

3.2. Stress measurement

The residual stress measurements were performed using a Jeol Ω-goniometer with a position sensitive detector (PSD). The X-ray radiation used was CuK_α, where the diffraction angle for the peak Al (422) is $2\theta = 137.45°$. Seven ψ angles between -40 and $40°$ were used, evenly distributed in $\sin^2\psi$, combined with three Φ angles, 0°, 45° and 90°, i.e. all in all 21 measurement angles, in order to make three-dimensional analysis possible. For a definition of the above angles, see [2].

The diffraction peak positions were determined by least squares fitting of a pseudo Voigt function to the measured peaks [19]. The K_{α_1} and K_{α_2} peaks were both used in the fitting procedure, and the fitting parameter for the K_{α_1} peak was taken as the peak position. The pseudo Voigt function is the sum of a Gaussian and a Lorentzian function, where the fraction of each function type is a parameter. In addition to peak position and intensity, it also has the peak width and angular separation between the K_{α_1} and K_{α_2} peaks as parameters. The computer programs used for peak analysis and stress calculations have been developed by Persson [20].

Measurements were confined to the matrix, since the reflections from the reinforcement phase were too weak to give any useful information. The penetration depth varies with the ψ angle between 70 μm for $\psi = \pm 40°$ and 103 μm for $\psi = 0°$ on the 95% level. It has been shown, [21], that a three-dimensional stress state develops in this kind of material at a depth below the surface of the same order as the interfibre or interparticle spacing. Since the interfibre spacing of the investigated composites is, by far, smaller than the penetration depth, surface gradients, i.e. gradients in the direction of the surface normal, can be neglected [21].

To make elevated temperature measurements possible, a special sample holder with a conduction heater was constructed [1]. The temperature was controlled with a Eurotherm controller, type 070. The thermocouple monitoring the temperature was positioned between the heating conductor and the specimen. A second thermocouple attached to the sample surface and connected to a single channel recorder showed temperature variations within ± 2 °C. Residual stress measurements have been made at temperatures between 25 and 250 °C. The diffraction angle 2θ given above is the theoretical room temperature value for pure aluminium. The lattice spacing and hence the diffraction angle changes with temperature due to thermal expansions as well as stress variations, and the PSD centre position has to be adjusted accordingly.

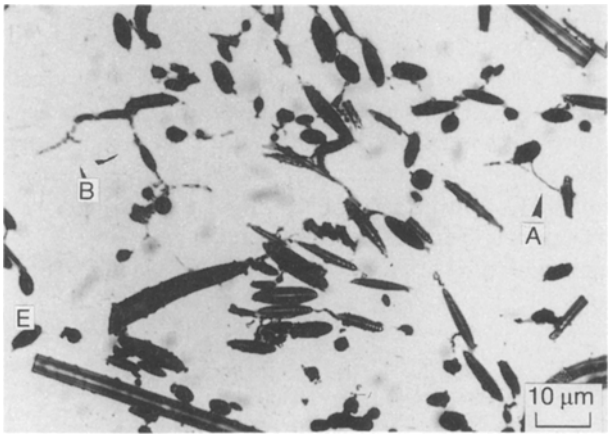

Figure 1 Microstructure of polished composite with 20 *v/o* fibres. Arrows A and B indicate transformed binder and Mg_2Si, respectively.

3.3. Eshelby modelling

The thermally induced residual stresses can be easily modelled following the Eshelby approach as described above. The parameters taken into account in the model are the elastic constants and coefficients of thermal expansion of the phases, and the volume fraction and shape, i.e. aspect ratio, of the inclusion. Relevant values of these parameters are given in Table I.

Material	Young's modulus (GPa)	Poisson's ratio	CTE (10^{-6} K^{-1})	Vol. fraction (%)	Aspect ratio
Al–2Mg	70[a]	0.33[a]	25.6[a]	Balance	–
Al_2O_3	300[b]	0.26[c]	7[b]	10, 20, 26	4

[a] Reference [22] for the alloy AA 5050.
[b] Reference [23].
[c] Reference [24].

4. Results and discussion

4.1. Unstressed lattice spacing

It is essential that the diffraction angle $2\theta_0$, corresponding to the unstressed lattice spacing be accurately determined, since the stress values of the residual stress tensor are strongly and directly dependent on the shift, $\Delta 2\theta = 2\theta - 2\theta_0$, between the measured diffraction angle, 2θ, and the unstressed value, $2\theta_0$. The value $\Delta 2\theta$ is normally small, and hence even a small error in the determination of $2\theta_0$ will cause a large error in the stress results.

The reaction between magnesium from the matrix and silicon from the silica in the fibres described in Section 3.1. and shown in Fig. 1 affects the 2θ values and is clearly revealed by X-ray diffraction measurements; powders made from materials with different fibre volume fractions do not all have the same lattice spacing. The reason is that magnesium has a strong effect on the lattice parameter of aluminium. According to [25], each per cent of Mg added to Al increases the lattice parameter by 0.0005 nm. Hence, the depletion of Mg from the matrix due to formation of spinel ($MgAl_2O_4$) and Mg_2Si precipitates is readily seen by a reduction in plane spacing, or rather by a shift to larger 2θ values. Clearly, powder made from an unreinforced matrix alloy or from composites with either fibre volume fraction is not sufficient to establish a relevant stress-free reference. Consequently, all powders were measured at all measurement temperatures at short intervals throughout the work. However, no significant difference between the diffraction angles of the powders with 20 and 26 *v/o* fibres was found, which indicates that 20 *v/o* fibres contain enough Si to reduce the Mg content of the matrix to a minimum.

The dependence of powder diffraction angle, $2\theta_0$, on measurement temperature for the different fibre volume fractions is shown in Fig. 2. Such measurements on stress free powders also provide a check on the alignment of the goniometer. Any misalignment or sample displacement, etc., is immediately revealed by the $2\theta_0$ measurements.

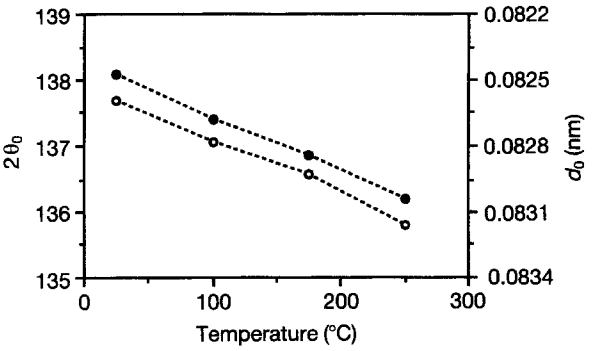

Figure 2 Diffraction angle, $2\theta_0$, and lattice spacing, d_0, as a function of measurement temperature for stress-free powders with (○) 10% and (●) 20 and 26% fibre volume fraction.

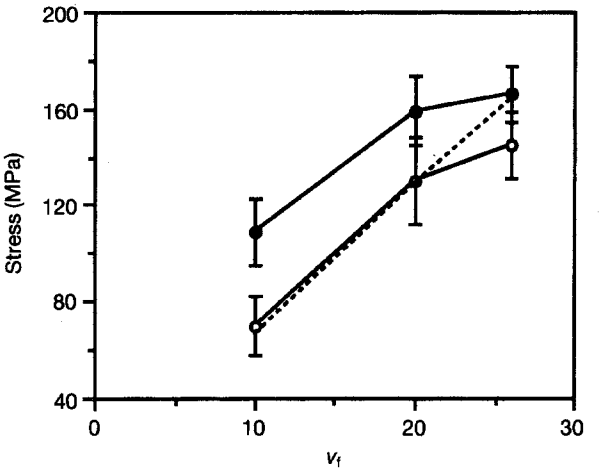

Figure 3 Measured (——) and predicted (- - -) residual stresses at 25 °C as a function of fibre volume fraction, v_f, for samples cut (○) parallel (x–y) and (●) perpendicular (x–z) to the original fibre plane. Error bars indicate one standard deviation.

4.2. Residual stresses

The measured residual stresses are in all cases, as expected, tensile in the matrix. Since the fibre are randomly distributed in a plane (referred to as the x–y plane) in the preforms, the stress directions σ_x and σ_y are geometrically identical and different from the σ_z direction. However, when pressure is applied during casting the fibres are redistributed somewhat, and the deviation from a totally random distribution of fibres in the final composites is small. Hence, no significant difference in residual stress values between directions within a sample is found. From this and the fact that the average shear stresses are exceedingly small, it can be deduced that a hydrostatic state of stress is present. Hence, only the hydrostatic matrix stress, $\sigma = (\sigma_x + \sigma_y + \sigma_z)/3$, is shown in the figures here and discussed in the following. The measured stress values at 25 °C shown in Fig. 3 increase with increasing amounts of reinforcing phase in accordance with Eshelby calculations. Even though measured stress values *within* a sample are the same regardless of stress direction, i.e. $\sigma_x = \sigma_y = \sigma_z$ within errors, they may differ *between* samples as seen in Fig. 3. The dashed line in the figure is the prediction of the stress after

cooling from the annealing temperature (350 °C) to the measurement temperature using the Eshelby model for equivalent inclusions.

Measurements at elevated temperatures also show that the stresses decrease as the temperature is increased. Results from measurements at four different temperatures between 25 and 250 °C are shown in Fig. 4 for the three fibre volume fractions. As before, calculated stresses are indicated by dashed lines. The calculations predict larger stresses for larger temperature drops, i.e. at lower measurement temperatures. Measurements confirm this trend, and the experimentally obtained stress values are in good conformity with calculations.

Comparing the predicted and measured stresses in Fig. 4 it is interesting to note that the difference between calculated and experimentally obtained values seems to increase with increasing fibre volume fraction. This is more easily seen in Fig. 5, where the difference between calculated and measured stress is shown as function of fibre volume fraction. Except for the "misbehaving" 20 *v/o* composite at 175 °C the general trend is clear; for low fibre volume fractions the difference is small or even negative, whereas larger positive values result at $v_f = 26\%$. Since no plasticity is taken into account in the Eshelby model, these results indicate that the composite's behaviour during slow temperature changes is largely elastic for the two lower fibre volume fractions, while some plastic yielding has occurred in the 26 *v/o* case. In [11] it is suggested that local flow can occur, resulting in microplasticity, and from calculations by Persson and Ohlsson [26] it is clear that yielding occurs locally in stress intense areas, e.g. around fibre ends.

The good bonding at the fibre–matrix interface [18] imposes mutual constraints on the phases during temperature changes, but if the amount of reinforcing phase and/or the temperature drop is large the matrix can no longer accommodate the large strains, whence yielding occurs. This behaviour has previously been found during thermal cycling with water or liquid nitrogen quenching of the same material [27]. Upon yielding, dislocations move in directions governed by the local stress fields they experience. Since the local stress fluctuations average to zero [8] they do not aid dislocation movement in any particular direction. It follows that no macroscopic flow occurs due to the local stress fields [11]. Rather, the flow that contributes to the stress reduction is directed by the average microstress. For low fibre volume fractions the yield stress of the matrix is not surpassed, and no yielding occurs.

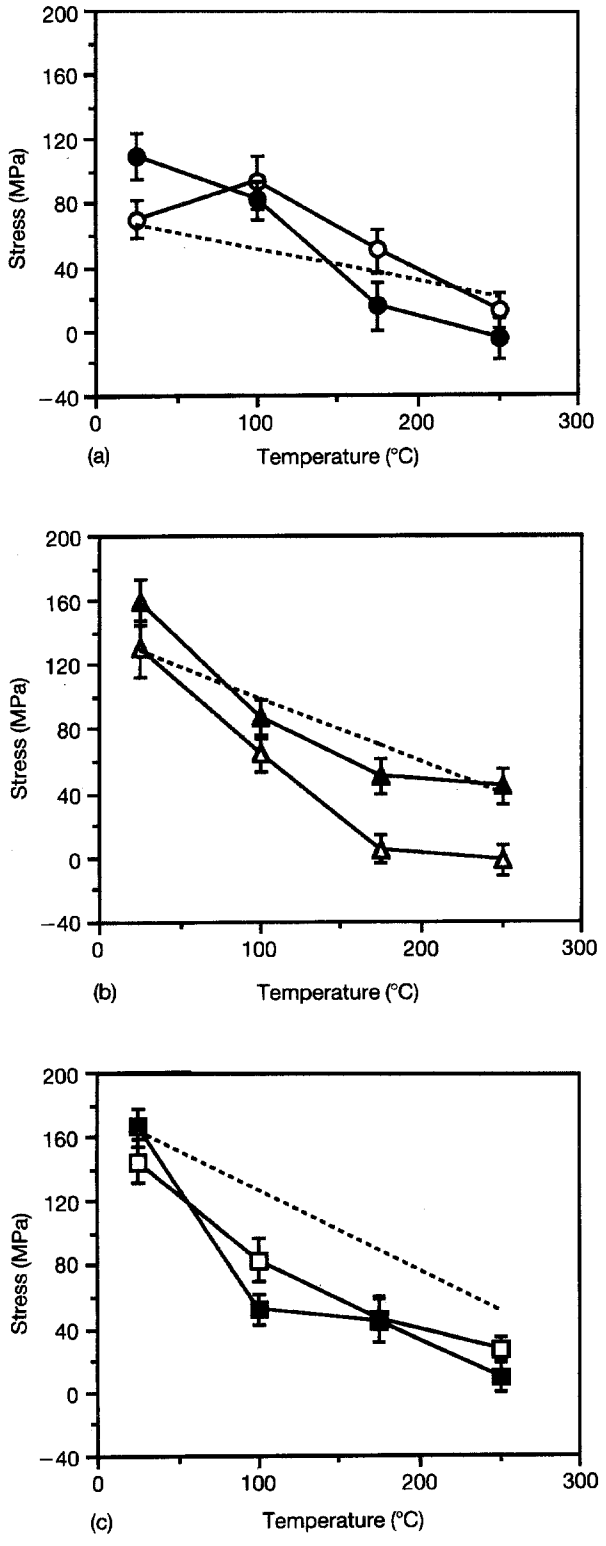

Figure 4 Measured (——) and predicted (- - -) stresses at different temperatures for samples cut (○, △, □) parallel (x–y) and (●, ▲, ■) perpendicular (x–z) to the original fibre plane with fibre volume fractions: (a) 10%, (b) 20%, and (c) 26%. Error bars indicate one standard deviation.

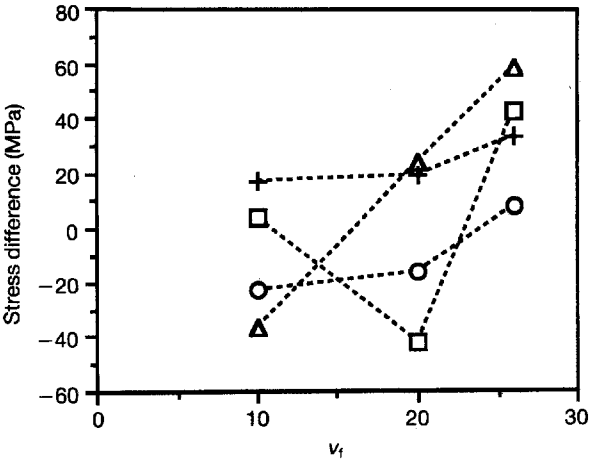

Figure 5 Stress difference (predicted minus measured stress) at (○) 25, (△) 100, (□) 175 and (+) 250 °C as a function of fibre volume fraction, v_f.

4.3. Plastic behaviour

The elastic–plastic behaviour of the matrix is considered in the following. During temperature changes the behaviour of an MMC can be modelled as the expansion or contraction of a rigid cavity in an elastic–plastic matrix, and the resulting equations can be solved analytically for simple geometries. Let us consider the composite as a system of fibres as spherical shells with radius, a, in a surrounding matrix shell with radius, b, which can be plastically deformed. The radii, a and b, are defined by the mean fibre size and the volume fraction of fibres, v_f, so that $v_f = a^3/b^3$. Following Hill [28] and Pickard and Derby [29], and considering that Young's modulus, as well as yield stress, vary with temperature, the critical temperature change, ΔT^*, required to initiate full plastic flow can be calculated from

$$\Delta T^* = |T_1 - T_2| = \frac{\sigma_0(T_0 - T_2)(1 - v)}{\Delta\alpha T_0 E^*(1 - C_1 T_2)v_f} \quad (5)$$

where T_1 is the initial and T_2 the final temperature and σ_0 and T_0 are constants. For this material, $\sigma_0 = 65.8$ MPa and $T_0 = 595\,^\circ$C [1].

Solving for T_{2_c}, i.e. the temperature at which full plastic yielding initiates on cooling from $T_1 = 350\,^\circ$C, the yield temperatures T_{2_c} arrived at are given in Table II. For the two larger fibre volume fractions this model predicts that the matrix behaves plastically during a large proportion of the cooling down to room temperature. The experimental data clearly support this elastic–plastic behaviour for the highest fibre volume fraction since the difference between predicted and measured stress values is positive, cf. Figs 4 and 5. In the case of 20 *v/o* fibres the difference between measured values and the elastic (Eshelby) prediction is smaller and agreement with the model is more uncertain than for the 26 *v/o* material, cf. Fig. 5. It should be pointed out that the intervals of measured stress given in Table II include all components of stress tensor and also comprise occasional values deviating from typical ones.

Equation 5 can also be used to predict the onset of plastic yielding during the temperature increase from 25 °C to measurement temperature. These values, T_{2_h}, are also shown in Table II. The observed decrease in residual stress at elevated temperatures is hence predicted to be elastic and reversible up to T_{2_h} in Table II. It is, however, important to note that T_{2_h} specifies the temperature for initiation of *full* plastic yielding. Due to the lower dislocation density between fibres than adjacent to fibres, the matrix is weaker between fibres, implying that plastic deformation begins between fibres before the entire matrix yields plastically [7]. Hence, one can assume that local yielding has occurred before the temperature, T_{2_h}, is reached.

Comparing the values of T_{2_h} with the levelling-out temperatures of the stress versus temperature curves in Fig. 4, it is seen that stress-decreasing mechanisms have indeed been active below T_{2_h}, but additional experiments are needed to determine the relative amount of reversible and irreversible stress relaxation and will be the aim of future work.

In the case of $v_f = 10\%$ the predicted temperature, T_{2_h}, in Table II is above the maximum measurement temperature, but as shown in Fig. 4a the stresses decrease with increasing temperature at least up to 250 °C. This relaxation is hence interpreted as largely elastic.

Even though the absolute values of the stresses are somewhat different between the x–y and x–z directions for the composite with $v_f = 20\%$, the temperatures at which plateaux are found in the stresses versus temperature curves of Fig. 4b are the same namely 175 °C. Comparing with the predicted temperature for onset of full plastic yielding $T_{2_h} = 171\,^\circ$C, it is found that the elastic, and to some extent plastic, mechanisms active below T_{2_h} have been rather effective, in as much as only minor stress changes are found above 175 °C.

The results for the highest v_f material shown in Fig. 4c seem to agree with the theoretical value $T_{2_h} = 141\,^\circ$C, in so far as the levelling-out of the stress versus temperature curves occurs at a lower temperature for this fibre volume fraction than for the two lower v_f composites. For this high fibre volume fraction, further stress relief through plastic relaxation occurs above T_{2_h} where the elastic limit is reached.

Interpreting the results from the elastic–plastic predictions, one should bear in mind that the considerations presuppose that the rigid cavity be spherical, and that interaction between cavities (fibres) is not taken into account. The influence of fibre interaction on the relaxation behaviour increases of course as the interfibre spacing decreases, i.e. as the fibre volume fraction increases. Furthermore, being largely ellipsoidal or cylindrical, the fibres impose other constraints on the matrix than do spherical inclusions such as particles, undoubtedly affecting the elastic–plastic behaviour of the matrix.

TABLE II Predicted and measured matrix stresses, σ_m, after cooling from 350 to 25 °C, and calculated yield temperatures during cooling and heating for different fibre volume fractions

Fibre volume fraction	σ_m^a (MPa) Predicted	σ_m^b (MPa)	Yield temperature, $T_{2_c}^c$ (°C)	Yield temperature, $T_{2_h}^d$ (°C)
0.10	67	67–119	39	280
0.20	129	125–176	231	171
0.26	164	142–182	269	141

[a] Eshelby model.
[b] The intervals include all stress components in samples cut in (x–y) as well as (x–z) direction.
[c] On cooling.
[d] On heating.

5. Conclusions

From the present work the following conclusions can be drawn:

1. A device enabling residual stress measurements at elevated temperatures using X-ray diffraction has been constructed and used to measure thermal residual stresses in Al-based composites at temperatures up to 250 °C.

2. The lattice spacing in the matrix is strongly dependent on the volume fraction of fibres due to reactions between the fibre surface and the matrix alloy during production. An accurate determination of the diffraction angle, $2\theta_0$, corresponding to the unstressed lattice spacing hence necessitates measurement on powders made from composites with all different fibre volume fractions.

3. The residual stresses are all tensile in the matrix, and the deviation from a hydrostatic stress state is very small. The stresses show a strong dependence on temperature as well as fibre volume fraction. From values of typically 130 MPa at room temperature they decrease with increasing temperature, approaching zero at the maximum measurement temperature.

4. The Eshelby model for equivalent inclusions is a powerful tool in predicting thermal stresses. However, being an elastic model, the discrepancy between experiments and predictions becomes evident for high fibre volume fractions, where the proportion plastic behaviour of the matrix during temperature changes is significant.

5. The stress reduction that occurs in the composites at elevated temperatures is a combination of elastic (reversible) and plastic (irreversible) relaxation that can be described using elastic theory and a model based on a rigid cavity in an elastic–plastic matrix.

Acknowledgements

The authors are greatly indebted to Lic. Eng. Christer Persson for several valuable suggestions and discussions and for supplying computer programs for peak evaluation and stress calculation. Helpful discussions and advice from Professor Thomas Johannesson are gratefully acknowledged, as is Dr Bengt Hildenwall for his comments on the manuscript. The work was financially supported by NUTEK (the Swedish Department for Industrial and Technical Development, formerly STU) as part of a programme of work on metal matrix composites.

References

1. A. OHLSSON, in "Thermal Residual Stresses in Metal Matrix Composites – Elevated Temperature Measurements and Heat Treatment Effects", Linköping Studies in Science and Technology, Licentiate Thesis No. 269 (1991).
2. I. C. NOYAN and J. B. COHEN, in "Residual Stress" (Springer Verlag, Berlin, 1987).
3. L. CASTEX, J. M. SPRAUEL, M. BARRAL, J. L. LEBRUN, G. MAEDER and S. TORBATY, in "Proceedings of the 21st Symposium on X-ray Stress and Mechanical Behaviour of Materials" Society for Material Science, Kyoto, 1984.
4. J. D. ESHELBY, *Proc. R. Soc.* **241A** (1957) 376.
5. *Idem, ibid.* **252A** (1959) 561.
6. *Idem, Prog. Solid Mech.* **2** (1961) 89.
7. R. J. ARSENAULT and M. TAYA, *Acta Metall.* **35** (1987) 651.
8. L. M. BROWN and W. M. STOBBS, *Phil. Mag.* **23** (1971) 1185.
9. O. B. PEDERSEN, in "Proceedings, IUTAM Eshelby Memorial Symposium, edited by B. A. Bilby, K. J. Miller and J. R. Willis (Cambridge University Press, 1985) p. 129.
10. P. J. WITHERS, D. J. JENSEN, H. LILHOLT and W. M. STOBBS, in "Proceedings, ICCM VI," edited by F. L. Matthews, N. C. R. Buskell, J. M. Hodgkinson and J. Morton (Elsevier Applied Science, 1987) p. 2, 255.
11. P. J. WITHERS, W. M. STOBBS and O. B. PEDERSEN, *Acta Metall* **37** (1989) 3061.
12. M. TAYA, K. E. LULAY and D. J. LLOYD, *Acta Metall. Mater.* **39** (1991) 73.
13. M. ODÉN, in "Residual Stress in Ceramics and Ceramic Composites", Linköping Studies in Science and Technology. Licentiate Thesis No. 329 (1992).
14. T. MURA, in "Micromechanics of Defects in Solids" (M. Nijhoff Publisher, Dordrecht, 1982).
15. M. TAYA and R. J. ARSENAULT, in "Metal Matrix Composites, Thermomechanical Behavior" (Pergamon Press, Oxford 1989).
16. Z. Li, PhD Thesis, University of Washington, 1988.
17. J. DINWOODIE, E. MOORE, C. A. J. LANGMAN and W. R. SYMES, in "Proceedings, ICCM V", San Diego, CA (1985).
18. Z-K. LIU, J. ÅGREN and A. MELANDER, *Mater. Sci. Engng* **A135** (1991) 125.
19. S. A. HOWARD and K. D. PRESTON, in "Reviews in Mineralogy, Modern Powder Diffraction", Vol. 20, edited by D. L. Bish and J. E. Post.
20. C. PERSSON, in "Residual Stresses in Metal Matrix Composites after Plastic Straining and Thermal Cycling", Linköping Studies in Science and Technology, Licentiate Thesis No. 332 (1922).
21. T. HANABUSA, K. NISHIOKA and H. FUJIWARA, *Zeitschrigt Metallkunde* **74** (1983) 5.
22. "Metals Handbook," Vol. 2, 9th Edn., (American Society for Metals, Metals Park, OH, 1979).
23. R. WARREN, in "17th CIMAC Conference" Warsaw (1987).
24. D. W. RICHERSON, in "Modern Ceramic Engineering" (Marcel Dekker, New York, 1982).
25. L. F. MONDOLFO, in "Aluminium Alloys: Structure and Properties" (Butterworth, 1976), p. 313.
26. C. PERSSON and A. OHLSSON, unpublished results (1992).
27. A. OHLSSON, C. PERSSON and T. ERICSSON, in "Proceedings of the Third European Conference on Residual Stresses, Frankfurt, November 1992," edited by V. Hauk, H. P. Hougardy, E. Macherauch and H-D. Tietz (DGM Informationsgesellschaft mbH, Oberursel, 1993) p. 593.
28. R. HILL, in "The Mathematical Theory of Plasticity" (Oxford University Press, 1953).
29. S. M. PICKARD and B.DERBY, *Acta Metall Mater.* **38** (1990) 2537.